Nickel Carbide (Ni3C) Nanoparticles for Catalytic Hydrogenation of Model Compounds in Solvent

Rémi André, Léna Meyniel, Sophie Carenco

Nickel Carbide (Ni_3C) Nanoparticles for Catalytic Hydrogenation of Model Compounds in Solvent

Rémi F. André,[1] *Léna Meyniel,*[1] *Sophie Carenco,*[1,*]

[1] Sorbonne Université, CNRS, Collège de France, Laboratoire de Chimie de la Matière Condensée de Paris (LCMCP), 4 place Jussieu, 75005 Paris, France

*Corresponding author. E-mail: sophie.carenco@sorbonne-universite.fr

Abstract:

Finely divided nickel is one of the main heterogeneous catalysts for liquid phase hydrogenation of nitro and alkyne moieties. However, it constitutes a major safety hazard due to its pyrophoric character and may be subject to poisoning issues, which can be overcome by the use of alternative nickel-containing phases. We investigated here crystalline nickel carbide nanoparticles (NPs) as catalyst in colloidal suspension for hydrogenation reactions under H_2 (7 bar) and below 100 °C. The Ni_3C NPs catalyst was prepared by thermal decomposition of $Ni(acac)_2$ at 250 °C in a mixture of oleylamine and 1-octadecene, and characterized by X–Ray Diffraction (XRD) on powder, Transmission Electron Microscopy (TEM) and X–Ray Absorption Spectroscopy (XAS). Polar solvents appeared comparatively more favorable than less polar ones for the hydrogenation of two model substrates: nitrobenzene and phenylacetylene. Furthermore, the presence of water in the solvent mix was mostly favorable to the hydrogenation yield. Considering the known metastability of Ni_3C at elevated temperatures (> 300 °C), TEM, XRD, XAS and X–ray Photoelectron Spectroscopy (XPS)

were used to verify the structural integrity of the Ni_3C phase and the evolution of the NPs surface upon catalysis. Complementarily, we confirmed that the nanoparticles are the active catalytic species and not leached species. Lastly, we expanded the scope to a variety of aldehydes, ketones, esters, nitriles and unsaturated hydrocarbons. Altogether, this study highlights the relevance of Ni_3C, a catalytic phase so far overlooked for these hydrogenation reactions.

Keywords: hydrogenation, nickel carbide, nanoparticles, colloidal catalysis, liquid-phase heterogeneous catalysis

1. Introduction

In fine chemistry, hydrogenation reactions are crucial steps for the production of various chemicals, such as pharmaceuticals, agrochemicals, fragrances or dyes. Typical substrates include polar functional groups (nitriles, nitro and carbonyl compounds) or unsaturated hydrocarbons (alkenes, alkynes).[1–4] The most efficient heterogeneous catalysts for these reactions are generally based on platinoid elements (Pd, Pt, Ir…) but their scarcity and high prices are problematic if industrial applications are envisioned.[5] In 1927, Murray Raney developed a nickel-aluminum alloy susceptible to form a "spongy" nickel phase presenting high specific surface: the famous Raney® catalyst.[6] This catalyst has proved its efficiency for the hydrogenation of organic molecules and is widely used in diverse fields of industrial catalysis.[7] The use of finely divided metallic nickel finds nonetheless limitations in its high reactivity to air, rendering it pyrophoric and therefore delicate and hazardous to handle on large scales, with a few reports of incidents in industrial sites.[8] Besides, such an active nickel catalyst is sensitive to poisoning and has a limited chemoselectivity in absence of co-catalyst.[1]

During the past decades, the search for new active phases for liquid-phase hydrogenations has therefore attracted interest, in particular regarding nanoparticles of compounds of abundant transition metals (Fe, Co, Ni, Cu), recently reviewed by Beller *et al.*[3] In order to promote the use of these metals, a modification of their electronic properties by insertion of light elements (*e.g.* boron, nitrogen, phosphorus) was considered. Such a modification of the metal phase lowers the metallic character of the material and increases its iono-covalent one, which may result in an improvement of the catalytic activity and/or of the chemoselectivity.[3,9] Accordingly, the use of nickel phosphides (Ni_2P, $Ni_{12}P_5$, Ni_5P_4) nanoparticles (NPs) was reported for catalytic batch hydrogenation of cinnamaldehyde (120 °C, 30 bar H_2 in cyclohexane),[10] of phenylacetylene and styrene (85 °C, 6 bar H_2 in dioxane),[11] of nitroarenes (80 °C, 10 bar H_2 in EtOH),[12] and of sugars (100 °C, 1 bar H_2 in

H_2O).[13] In particular, Corma *et al.* reported a considerable improvement of the chemoselectivity of Ni_2P compared to Ni(0) for the semi-hydrogenation of phenylacetylene.[11] Among different published works, there are also mentions of the use of nickel sulfides, from NiS_2 to Ni_4S_3, for nitroarenes (110–150 °C, 30–40 bar H_2 in MeOH or EtOH),[14,15] of nickel nitride, Ni_3N, for alkynes (100 °C, 20 bar H_2 in EtOH),[16] of nickel silicide, Ni_2Si, for a large scope of reducible molecules (40–130 °C, 10–50 bar H_2 in H_2O/MeOH),[17] and of nickel borides for nitrobenzene (65 °C, 4 bar H_2 in MeOH).[18] Altogether, these works highlight the opportunities to unravel for hydrogenation reactions by exploring alternative compositions of nickel containing a lighter element. There is however, to the best of our knowledge, no mention of nickel carbide for hydrogenation reactions under soft conditions. Only one work, led by Assamburungrat *et al.*, mentions the use of nickel carbide (NiC) for the hydroprocessing of coffee oil under harsh conditions (400 °C, 20–40 bar H_2), with an interestingly higher catalytic activity observed for NiC than for NiS and NiP.[19] The other works with nickel and carbides concern the use of bimetallic ones, such as Ni–Mo–C and Ni–W–C, for hydrogenation of various substrates including nitroarenes,[20] m-cresol,[20] anisole,[21] ethyl caprate,[21] and furfural,[22,23] also under relatively strong reaction conditions (120–320 °C, 20–65 bar H_2). In this context, it seems relevant to investigate the most common nickel carbide phase, hcp-Ni_3C, under the form of well-defined nanoparticles. Nickel carbide (Ni_3C) indeed raised interest these past years for applications in electrocatalysis (oxygen evolution reaction,[24–26] hydrogen evolution reaction[25–27]), photocatalysis,[28] and dry reforming of methane,[29] but not yet for H_2 activation.

The present work thus reports the use of Ni_3C NPs for batch liquid-phase hydrogenation reactions in mild conditions, *i.e.* below 100 °C and 10 bar of H_2, of a series of model substrates including styrene, phenylacetylene, nitrobenzene, benzaldehyde, acetophenone and benzonitrile. The evolution of the reactivity for phenylacetylene

hydrogenation was compared with Ni(0) NPs synthesized under similar conditions. The Ni_3C NPs catalyst was prepared by thermal decomposition of $Ni(acac)_2$ at 250 °C in a mixture of oleylamine (OAm) and 1-octadecene (ODE), and characterized by powder X–Ray Diffraction (XRD), Transmission Electron Microscopy (TEM) and X–Ray Absorption Spectroscopy (XAS). The structural integrity of the NPs and of their surface was assessed by TEM, XRD, XAS and X–Ray Photoelectron Spectroscopy (XPS).

2. Results and discussion

Ni_3C NPs synthesis and characterization. Briefly, both Ni(0) (used for comparison with Ni_3C) and Ni_3C NPs were prepared by thermal decomposition of nickel(II) acetylacetonate ($Ni(acac)_2$) according to the literature with modifications (see experimental section below).[30,31] Ni(0) NPs were obtained in pure oleylamine (OAm) at 220 °C. This last molecule, a high boiling point solvent, also plays the role of the reducing agent and of a ligand to stabilize the colloidal suspension. Ni_3C NPs were synthesized at higher temperature, 250 °C, in a mixture of OAm and 1-octadecene (ODE), this last one playing both the role of solvent and carbon source for the carbidization of the NPs (**Figure 1A**). The mixtures were let to react under N_2 for 2 h to generate black colloidal suspensions. The NPs powders were then recovered by addition of ethanol as counter solvent and centrifugation of the reaction crude.

The XRD patterns of the two samples indicate the materials are XRD-pure if compared with the references of fcc-Ni(0) [PDF card N° 03-065-2865] (**Figure S1**) and hcp-Ni_3C [PDF card N° 04-007-3753] (**Figure 1B**). The Scherrer analysis applied on peaks located at 2θ = 44.5°, 51.8° and 76.4° for Ni(0) indicates an average crystallite size of 23 nm. The same analysis applied on peaks located at 2θ = 39.5°, 41.9°, 45.0°, 59.0° and 71.8° for Ni_3C gives a value of 27 nm. Further investigation by TEM shows the formed NPs have similar morphologies with irregular shapes and are polydisperse in size, with diameters ranging from 50 nm to 100 nm (**Figure 1C-D** for Ni_3C NPs and **Figure S1** for Ni(0) NPs). Particles do not display privileged facets, they rather exhibit a variety of potential active sites. A dark contrast is observed between the NPs and the carbon background, which indicates the presence of heavy atoms such as nickel in their cores. The thickness of the NPs prevents the detection of electron diffraction fringes but the crystallinity of the sample is attested by the presence of spectral images of fairly large domains (**Figure S2**). Considering the size of the NPs observed by TEM (50 to 100 nm in diameter) *versus* the size of the crystallites according

to Scherrer analysis (*ca.* 25 nm), the NPs are polycrystalline. The light gray shell present at the surface of the objects is attributed to an organic layer due to the synthesis and the washing steps, any composition mapping would therefore be irrelevant as carbon is expected everywhere. Selected Area Electron Diffraction (SAED) performed on the sample confirmed the Ni_3C phase attribution by XRD (**Figure 1E**).

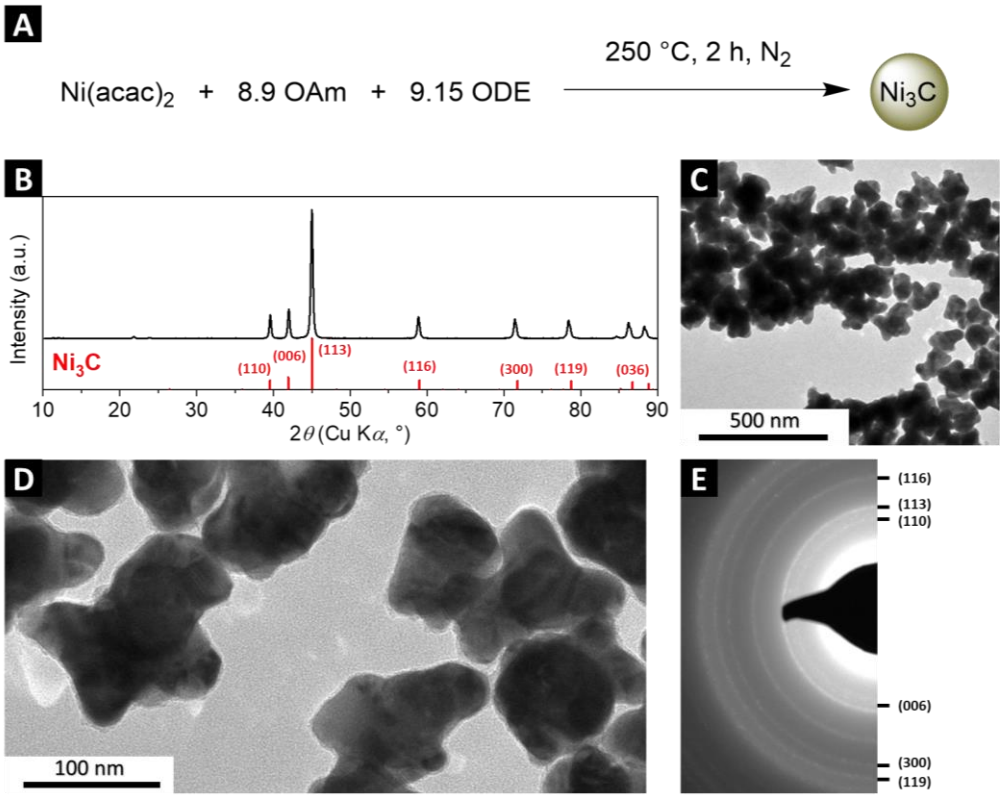

Figure 1. Nickel carbide nanoparticles formation and characterization. (A) Synthesis of nickel carbide nanoparticles, (B) XRD pattern (Ni_3C: PDF N°04-007-3753), (C-D) corresponding TEM images and (E) SAED pattern with (hkl) attributions.

Temperature choice in the synthesis of Ni_3C NPs. The precise temperature at which the carbide is formed was the object of several articles and depends on the reaction mixture concentration, on the temperature ramp, *etc*.[32] In this work, due to the presence of organic molecules at the surface of the NPs, the amount of carbon in the inorganic part cannot be accurately determined by elemental composition analysis. The Ni:C ratio is therefore estimated to be around 3 by XRD pattern matching. The nickel carbide phase, Ni_3C, can

however tolerate defects and should rather be considered as a solid solution of carbon in nickel Ni_3C_{1-x}. The solvothermal synthesis of Ni_3C NPs was first reported by Li *et al.* by thermolysis of nickel formate $Ni(HCOO)_2$ in a mixture of oleylamine and oleic acid.[33] This study was followed by Kobayashi *et al.* who used $Ni(acac)_2$ in OAm to form fcc-Ni(0) NPs and demonstrated the carbidization of the so-formed nanoparticles starts at *ca.* 240 °C.[34] The first stage of the Ni(0) NPs carbidization is challenging to observe with XRD and one can incorrectly assume pure metallic nickel was obtained, as demonstrated by Schaak *et al*.[32] It is important to note that no absolute decomposition temperature may be given for OAm, ODE, or any other carbon source, as the carbidization process is thermodynamically possible at low temperatures, *ca.* 200 °C, but is kinetically too slow to be observed.[32] For instance, in the Kobayashi's work, for a reaction time of 30 min, pure cubic Ni(0) was obtained until a reaction temperature of 260 °C and Ni_3C was observed at 280 °C and higher temperatures.[34] When the reaction was conducted at 240 °C, a longer reaction time (180 min *versus* 30 min) was enough to lead to Ni_3C formation. If solvents are compared as to their carbidization capacity, both the reaction temperature and reaction time should then be indicated. The exact decomposition mechanism of ODE is rarely mentioned in the different works. As higher temperatures are required for cardibizaton with OAm than with ODE, both comporting a C=C bond, we suggest the higher reactivity of ODE is linked to the terminal position of the double bond.

All these elements prompted us to clarify the conditions under which the nanoparticles were fully carbidized to Ni_3C in our experimental design. In this purpose, we investigated the phase speciation obtained at different reaction temperatures. When following the initial protocol published by Tracy *et al.* for Ni_3C NPs (reaction at 220 °C in OAm/ODE for 30 min),[30] the synthesis did not systematically provide XRD-pure Ni_3C NPs, as traces of fcc-Ni(0) were also observed (**Figure S3, b**). During the heating ramp toward 250 °C, a plateau in

temperature at *ca.* 236 °C was systematically observed, concomitant with explosions in the reaction crude, which may correspond to the carbizidation step. The reaction was therefore run and stopped right before (230 °C) or after (250 °C) this critical temperature of 236 °C and the crudes were treated and characterized by XRD as for the regular synthesis of Ni_3C NPs (**Figure S3, c-d**). When stopped at 230 °C, the reaction led to a mixture of Ni_3C (major phase) and Ni(0) (minor phase) while only Ni_3C was obtained when stopped at 250 °C. From these results, we propose that the critical temperature of 236 °C corresponds to a maximum rate of decomposition of ODE and endothermic carbon insertion in the nanoparticles. To avoid the leftover of some metallic phase, the reaction temperature was increased to 250 °C (30 °C higher than in Tracy's work) and the reaction time was increased to 2 h: this strategy was successful as XRD-pure hcp-Ni_3C NPs was then systematically obtained (**Figure S3, a**).

Crystallographic and electronic structure of Ni_3C. Nickel carbide is only known to crystallize in a hexagonal structure Ni_3C very close to that of hcp-Ni(0), with slightly larger lattice parameters. The carbon atoms occupy one third of the octahedral interstitial positions. The Ni(0) phase obtained in this study corresponds to the fcc-Ni(0), which is the most reported one for the catalytic studies. Ni K-edge X-ray Absorption Spectroscopy (XAS) was conducted on the Ni_3C NPs prepared at 250 °C to provide information on their electronic structure. It was compared with these of a nickel foil and of nickel oxide (NiO), as references. The analysis of the X–ray Absorption Near-Edge Structure (XANES) part of the spectrum reveals the shape of the edge and the intensity of the white line of the nickel carbide phase (Ni_3C) are close to those of metallic nickel (Ni(0) foil) (**Figure 2A**). For both materials, the position of the edge, *ca.* 8332 eV, is difficult to estimate due to the flat and stair-stepped pattern, covering the 8327–8352 eV range. This pattern may be explained by a complex density of states function, related to the nature of the bonds in the materials (**Figure 2B**). On the contrary, the NiO reference displays a shifted edge at 8344.8 eV and an intense white line,

in agreement with its strong ionic character. These results support the low oxidation state of the Ni atoms in Ni_3C and the metallo-covalent character of the phase. The coordination shells around the Ni atoms were further studied using the Fourier transform of the Ni K-edge Extended X–ray Absorption Fine Structure (EXAFS) oscillations. In the R-space spectra, one main peak at low distances is observed for Ni(0), centered at 2.19 Å, corresponding to a Ni–Ni bond (2.49 Å tabulated), and two for Ni_3C, centered at 1.50 Å and 2.35 Å, the second one corresponding to a Ni–Ni bond (2.63 Å tabulated) (**Figure 2C**). The Ni–Ni bond length increase from Ni(0) to Ni_3C is coherent with the slight expansion of the crystal lattice due to the carbon insertion. The small maximum observed at 1.50 Å for Ni_3C may be attributed to a Ni–C bond (1.86 Å tabulated), as suggested by Wokaun *et al.*,[35] although the interpretation of the very low distances in the R-space of the EXAFS spectra is delicate considering the issue of the phase uncertainty in EXAFS.[36] The systematic underestimation by *ca.* 0.3 Å in comparison with the crystallographic data is intrinsic to the EXAFS technique. Altogether, the XAS analysis indicates the electronic structure of the hcp-Ni_3C phase is still similar to that of fcc-Ni(0) with a slight increase of the Ni–Ni bond.

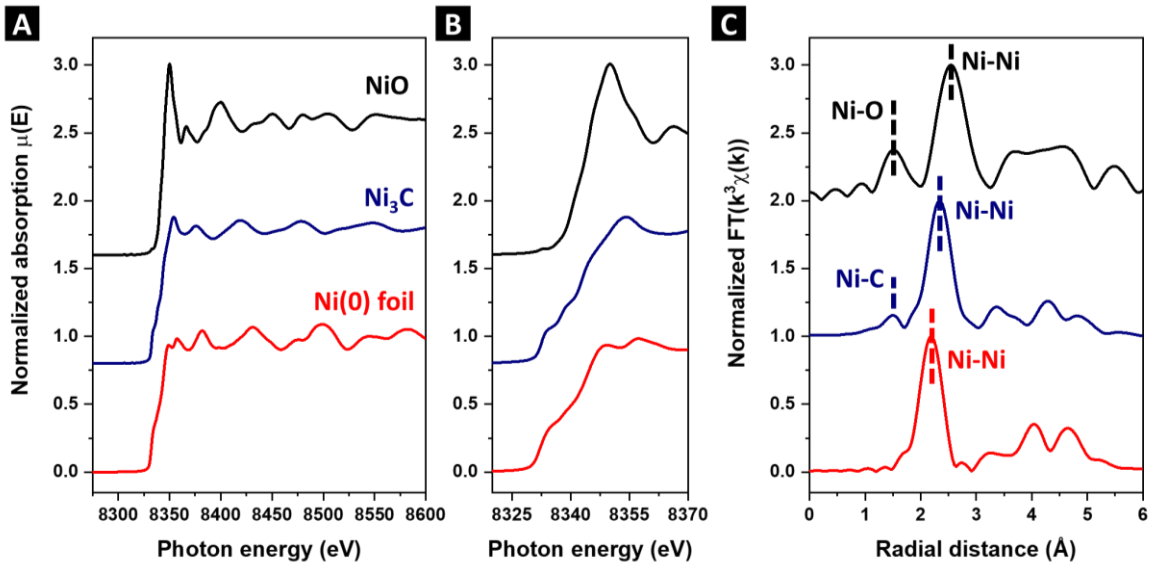

Figure 2. Electronic structure of Ni_3C NPs. (A-B) Normalized Ni K-edge X–ray absorption near-edge structure (XANES) spectra of Ni_3C NPs (blue) and of a Ni(0) foil (black) and NiO (red) as references, and (C) corresponding Fourier transforms k^3-weighted of EXAFS spectra in R-space.

Solvent effects. The use of the developed catalyst, Ni_3C NPs, was first demonstrated on two model reactions: the hydrogenation of nitrobenzene in aniline and the hydrogenation of phenylacetylene in styrene (STY) and ethylbenzene (EB). No conversion was obtained for the blank reactions conducted in ethanol at 100 °C in absence of catalyst. Then, the reduction was studied with Ni_3C NPs under mild reaction conditions (60 °C or 100 °C, 7 bar of H_2, 16 h). The catalyst loading is expressed in mol % [Ni] and corresponds to the total amount of nickel atoms introduced in the system, relative to the amount of substrate. The initial catalyst loading was of 10 mol % [Ni] (12.5 mg of Ni_3C NPs or 11.7 mg of Ni(0) NPs for 2 mmol of substrate). The number of exposed sites at the surface of the NPs is discussed later in the study. The studied solvents are representative of a wide range of polarity (*cf.* the Miller polarity indicated in brackets in the following list) and proticity: toluene (0.09), dioxane (0.16), 2-propanol (0.55), 1-butanol (0.59), 1-propanol (0.62) and ethanol (0.65).

At 100 °C, the conversion of nitrobenzene (in blue) was total whatever was the solvent (**Figure 3A**). At 60 °C, the conversion (in green) was lower at *ca.* 10 % for the less polar and protic solvents (toluene, dioxane, 2-propanol, 1-butanol, 1-propanol), but was still total for ethanol. The catalytic loading was then lowered to 1 mol % [Ni] and the reaction was conducted at 60 °C in ethanol: only 11 % of the nitrobenzene was converted in aniline. A similar trend was observed for the hydrogenation of phenylacetylene: full hydrogenation in ethylbenzene was observed in all alcohols at 100 °C (in dark blue) while only in 2-propanol and ethanol at 60 °C (in dark green) and merely no conversion in dioxane (**Figure 3B**).

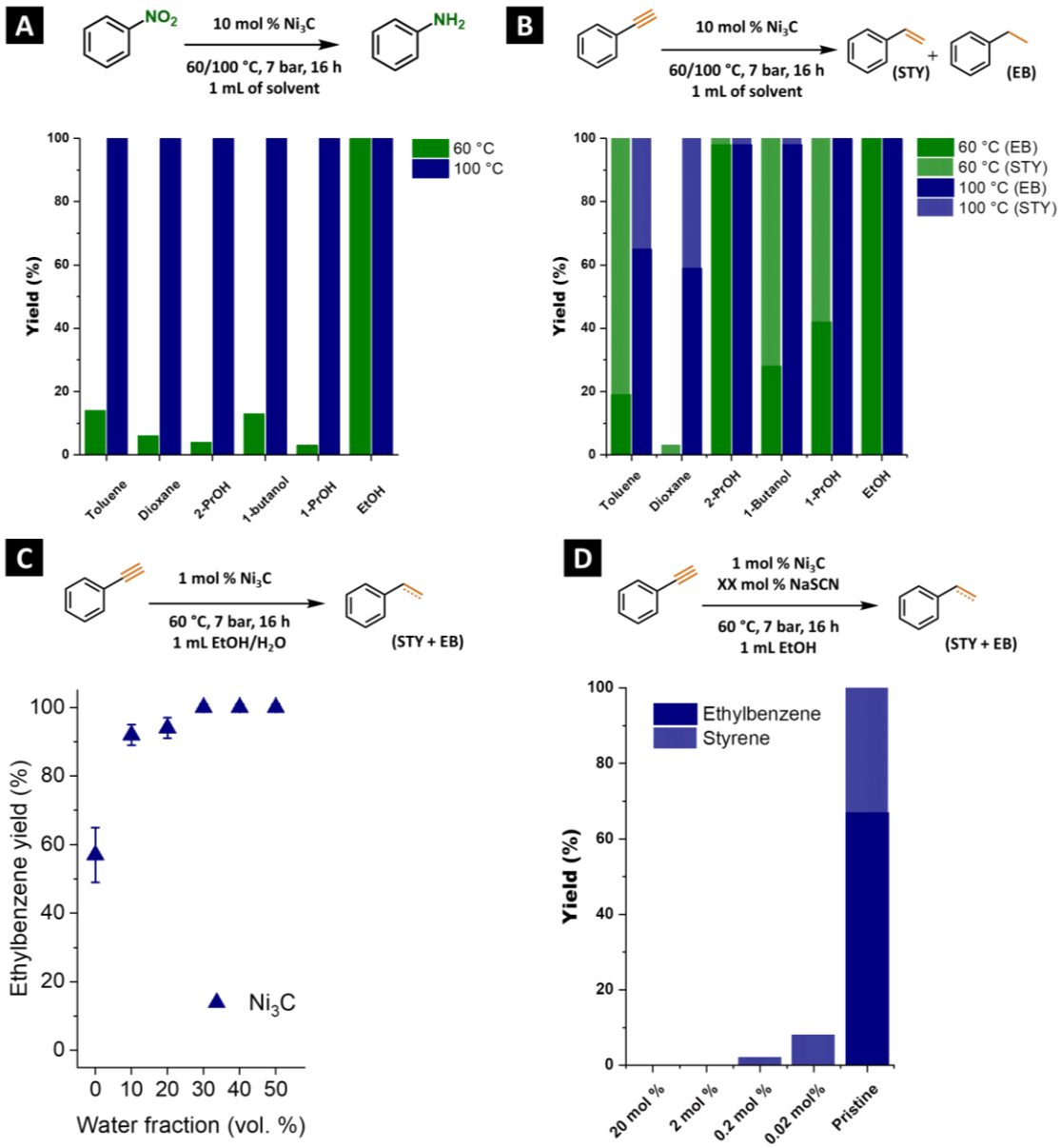

Figure 3. Hydrogenation reactions with Ni_3C nanoparticles. Reaction conditions: solvent (1 mL), substrate (2 mmol), Ni_3C NPs (12.5 mg, 10 mol % [Ni]), H_2 (7 bar), 16 h. (A-B) Influence of the solvent and of the reaction temperature on nitrobenzene hydrogenation in aniline and phenylacetylene hydrogenation in styrene (STY) and ethylbenzene (EB). (C) Influence of the addition of water in ethanol (volumic fraction). (D) Poisoning test with sodium thiocyanate (EtOH, 1 mol % [Ni], 60 °C). Yields determined by ^1H NMR.

Ethanol solvent may contain various amounts of water as an impurity. We thus decided, in an independent series of reactions, to add water on purpose. We therefore explored the impact of the water volume fraction on the ethylbenzene yield from phenylacetylene for the reaction performed in ethanol (**Figure 3C**). The yield increased from 57 % in absolute

EtOH (from the bottle on the bench) to 92 % in EtOH/H_2O (*v*/*v* = 8/1) and stayed high (> 90 %) even up to *v*/*v* = 1/1. It should be noted that phenylacetylene is hardly miscible with water and biphasic systems were obtained for water fraction higher than 20 % (*v*/*v* = 4/1). Moreover, the catalyst, surrounded by a shell of hydrophobic ligands, severely aggregated in the presence of water. Despite this, water was mostly beneficial to the ethylbenzene yield. In agreement with our observations, Beller *et al.* reported that the addition of water to dry THF increased the reaction rate for the nitroarene reduction by cobalt oxide catalysts.[37] This behavior was also reported by Guo *et al.* who demonstrated higher yields were obtained in EtOH/H_2O (*v*/*v* = 4/1) than in pure EtOH or pure H_2O.[38]

Solvents are known to impact the stability of reaction intermediates and transition states, mainly through their polarity or proticity, and thereby to affect the reaction rates and selectivities of reactions.[39] Moreover, light alcohols present hydrogen donating abilities which benefit hydrogenation reactions. The mechanism generally retained is the Meerwein–Ponndorf–Verley (MPV) one in which the alcohol used as solvent is transformed in aldehyde or ketone through the transfer of the β-hydrogen of the OH group to the bond to hydrogenate. Secondary alcohols thus form more stable products than primary ones, acetone in the case of 2-propanol for instance. Such an important impact of the reaction medium was for instance evidenced in the case of furfural hydrogenation on α-MoC catalyst for which the product yield increased from 11 % in cyclohexane to 96 % in methanol.[39] A similar explanation could be proposed to justify the higher reactivity observed in 2–propanol compared with 1-butanol or 1-propanol of similar polarities.

Paradoxically in our case, the best solvent for catalysis, ethanol, happened to be the counter-solvent of the NPs synthesis. The Ni_3C NPs then slowly aggregated during the course of the hydrogenation. This aggregation issue justified the use of independent reaction series,

with catalytic tests all originating from the same stock solution, in order to study the influence of a single parameter.

A leaching test was performed to evaluate whether the catalytic activity was actually due to the surface of the Ni_3C nanoparticles or to the formation of nickel complexes in solution (**Figure S4**), following a methodology already used on Cu and NiCo nanoparticles.[40,41] The nitrobenzene hydrogenation was performed in ethanol and the crude was centrifugated after reaction: the solid part was redispersed in a fresh ethanolic solution of nitrobenzene while fresh nitrobenzene was added to the liquid supernatant. After reaction overnight at 100 °C, no conversion was recorded for the supernatant while total hydrogenation was obtained for the reused Ni_3C NPs. The molecular species potentially produced by leaching of the NPs could therefore not be responsible for the catalytic activity.

We also checked the robustness of the catalyst stored in air. Indeed, contrarily to the classical Raney Ni, the Ni_3C NPs can be easily handled in air without safety hazard. The activity of the Ni_3C NPs catalyst remained high as total hydrogenation of nitrobenzene at 100 °C in ethanol was achieved with a 6-month-old catalyst.

Catalyst poisoning. On the basis of XAS, the nickel environment in Ni_3C resembles that of Ni(0), similar molecular adsorption and H_2 activation mechanisms may therefore be expected. A full DFT study is out of the scope of the present work but the similarities were assessed by poisoning tests. The surface poisoning of nickel catalysts by electronegative modifiers such as sulfur- or phosphorus-containing molecules is of high importance, as such poisoning agents are frequently found in reaction mixes. It must be highlighted the interactions between P/S and the metal atoms is of different nature in phosphides/sulfides and for poisoning: in the first case, the light element forms a iono-covalent bond with the metal, thereby modifying the electronic configuration of the whole material, whereas in the second

case, there is a coordination of molecules or ions at the surface of the catalyst, blocking or degrading metallic surface active sites. A particular attention has been devoted to the Ni (100) and Ni (111) surfaces by Goodman *et al.* and the authors report two mechanisms for the diminution of the catalytic activity through poisons: (a) a long-range electronic effect or "ligand effect" and (b) an ensemble effect.[42] In the first case, the deactivation is linked to the electronegativity of the poison and differences are expected between phosphorus and sulfur, for instance, at similar surface coverage. Furthermore, one poisoning atom is expected to deactivate several equivalent metal atoms (up to 10 in Goodman's study), explaining a dramatic drop in reactivity even at very low surface coverages (reaction rate divided by 10 at 0.05 sulfur monolayer). In the second case, the access to the metal centers is blocked by the poisoning agents and a more limited impact is expected as to the reaction rate.

Considering the similarities between fcc-Ni and hcp-Ni_3C previously mentioned as to the electronic structure, we expected similar poisoning mechanisms to take place for both phases and investigated the impact of a sulfur-based poison agent known for deactivating regular fcc-Ni. The sensitivity of Ni_3C NPs to the presence of sodium thiocyanate (NaSCN) was assessed at different concentrations (20 – 0.02 mol % *versus* the substrate) (**Figure 3D**). The catalytic activity was totally suppressed at 20 and 2 mol % but was significant at 0.2 and 0.02 mol % with respectively 2 % and 8 % of conversion of phenylacetylene, even though largely inferior to the quantitative conversion obtained without NaSCN. A rough estimation of the number of surface Ni atoms may be provided relying on geometrical considerations (**Figure S5**). Briefly, the "volume of surface atoms" is approximated considering an outer shell whose thickness is the metallic diameter of Ni (2.48 Å), to be compared with the total volume of the nanoparticle. The calculations give a percentage of surface atoms between 3.7 % and 1.5 % for respectively 40 nm and 100 nm large spheres. Considering the polydispersity of the samples and the poor sphericity of the NPs, we can estimate that *ca.* 2 %

of the nickel atoms of the Ni_3C NPs were accessible for catalysis. If the NPs were perfectly dispersed in the solvent, a 1:1 ratio for SCN^-:$Ni_{surface}$ would be obtained for the experiment at 0.02 mol % of NaSCN. The dramatic decrease in reactivity can then be interpreted as a strong poisoning of the reactive centers with a long-range electronic effect. This effect is similar to what was observed with classical fcc-Ni(0) sites, we therefore suggest the active sites here are of similar nature.

Comparison of the catalytic activity between Ni_3C and Ni(0) NPs. To further assess this idea, the hydrogenation of phenylacetylene was attempted with hcp-Ni_3C and fcc-Ni(0) NPs at lower temperatures and lower catalyst loadings (20-120 °C, 1 mol % [Ni]) (**Figure 4**). The two catalysts, synthesized with similar protocols, display similar morphological features and size of particles. However, a strong difference resides in their magnetism: the Ni(0) NPs mostly aggregate on the magnetic stirrer bar where Ni_3C NPs did not. No conversion was observed at 20 °C for neither Ni_3C nor Ni(0) NPs, but a quantitative conversion of phenylacetylene in styrene and ethylbenzene was reached at respectively 40 °C and 60 °C for both. The yield in ethylbenzene, the product of the total hydrogenation, reached *ca.* 90 % at respectively 80 °C and 100 °C. At similar catalyst loadings, Ni_3C NPs therefore display a comparable activity with Ni(0) NPs for the hydrogenation of phenylacetylene, with a similar chemoselectivity and dependence on temperature. The milder conditions required for phenylacetylene hydrogenation when compared with nitrobenzene were in line with other works reporting that the reduction of the unsaturated hydrocarbons is generally achieved at lower temperatures and H_2 pressures than that of polar groups such $–NO_2$.[17]

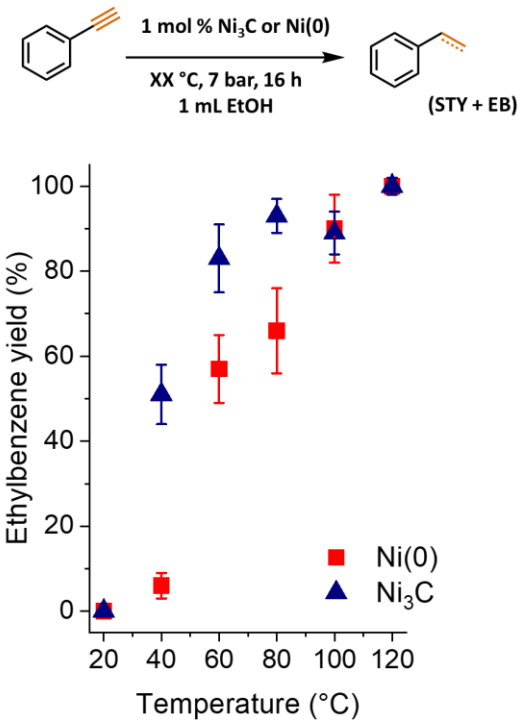

Figure 4. Low metal loadings experiments at different temperatures. Reaction conditions: ethanol (1 mL), phenylacetylene (2 mmol), catalyst (1.25 mg Ni_3C NPs or 1.17 mg Ni(0) NPs, 1 mol % [Ni]), H_2 (7 bar), 16 h. Yields determined by ^1H NMR.

The objective here is to explore the use of hcp-Ni_3C NPs as a hydrogenation catalyst instead of a purely metallic one. Rather than looking for a highly performing catalyst, a high importance was thus given to the purity of the phase, and the morphology of the NPs was not optimized regarding the accessibility to the metal sites. We nonetheless broadened the scope for the use of hcp-Ni_3C NPs in hydrogenation reactions in the next section.

Substrate scope. The hydrogenation of various compounds containing polar functional groups (aldehyde, ketone, enone, ester, nitro nitrile) or representative of the unsaturated hydrocarbons (alkyne, alkene), aromatic and aliphatic, was studied with a catalyst loading of 10 mol % [Ni] (**Figure 5**). At 100 °C, the conversion yields in alcohols were high for the three tested aldehydes (benzaldehyde, octanal and furfural), as well as for acetophenone. The conversion of benzophenone in benzhydrol was lower (36 %) and no

conversion was observed for butanone. *Trans*-cinnamaldehyde and *trans*-octenal were quantitatively hydrogenated in primary alcohols. A lower reactivity was nonetheless recorded for the chalcone, for which 40 % of the substrate was only partially hydrogenated in dihydrochalcone. As to esters, no conversion was observed for methyl benzoate nor ethyl caprate. The hydrogenation of benzonitrile led to a mixture of the secondary imine (N-benzyl-1-phenylmethanimine) and of dibenzylamine with a total consumption of the initial substrate. These two products resulted from the imine formation and self-condensation of the formed benzylamine. Following a strategy adopted by Beller *et al.*, significant amount of ammonia was added to the reaction crude ($[NH_3]$ = 7 mol.L^{-1} in $EtOH/H_2O$ (1/1)) in order to favor the total hydrogenation in benzylamine.[17] The high concentration in NH_3 indeed displaces the equilibrium of the two aforementioned reactions toward the benzylamine. Under these conditions, a quantitative transformation of butyronitrile in butylamine and of benzonitrile in benzylamine was obtained. As to nitro compounds, both nitrobenzene and p-nitrotoluene were quantitatively reduced in their corresponding amines, *i.e.* aniline and p-toluidine. Finally, in addition to styrene and phenylacetylene, which were fully hydrogenated in ethylbenzene, the 1-octene was hydrogenated in octane and the diphenylacetylene in a mixture of diphenylethane and stilbene, with a neat preference for the (Z) configuration. However, no conversion of naphthalene in tetralin was observed.

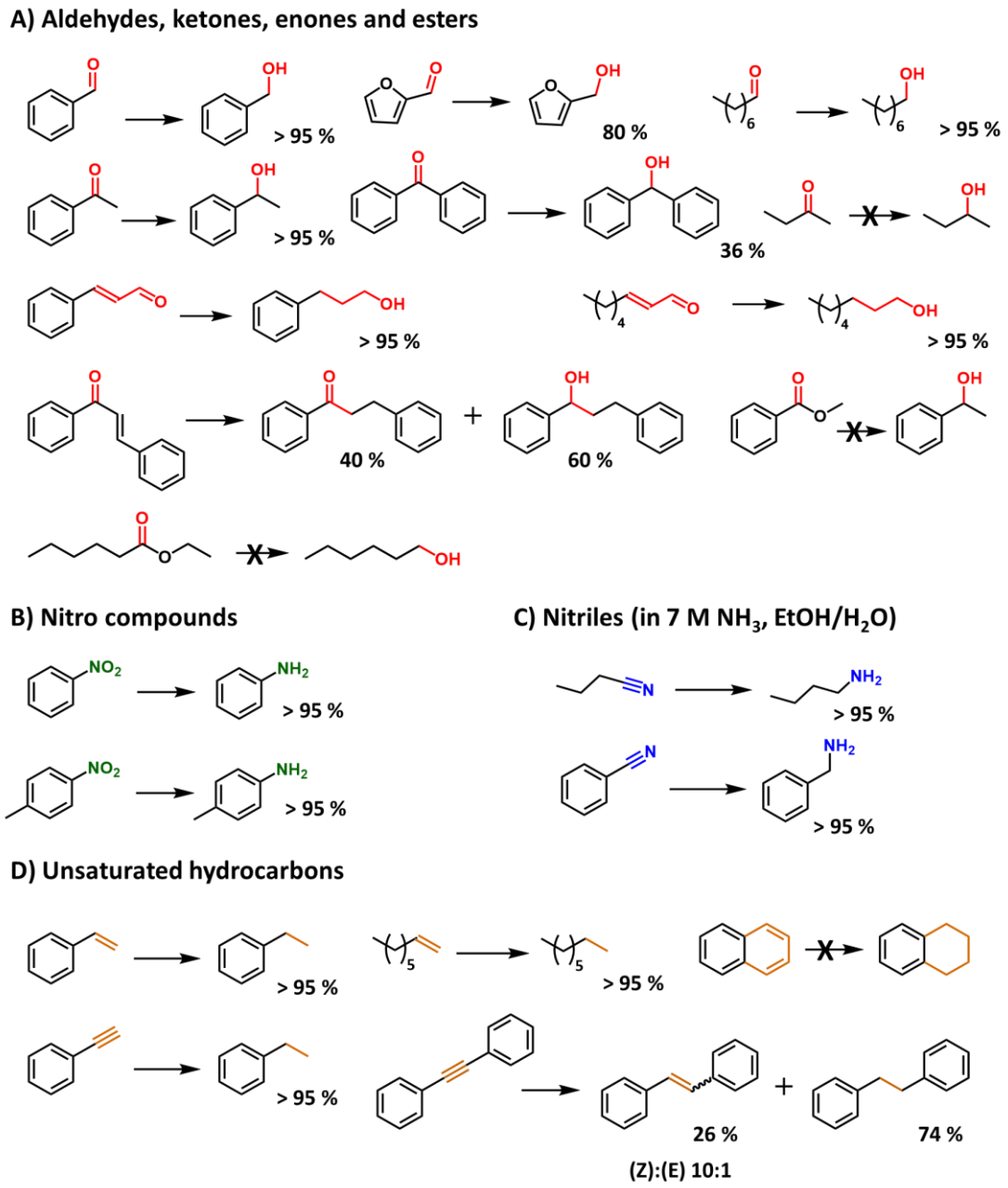

Figure 5. Substrate scope for the Ni_3C-catalyzed hydrogenation. Reaction conditions: Ni_3C NPs (12.5 mg, 10 mol % [Ni]), substrate (2 mmol), EtOH (1 mL), 7 bar H_2, 100 °C, 16 h, autoclave (25 mL).

Catalyst integrity. The structural integrity of the Ni_3C catalyst was finally assessed *post mortem* by means of TEM, XRD and XAS. In this purpose, hydrogenation of phenylacetylene was conducted in ethanol at 100 °C during 16 h and under 7 bar of H_2 with 10 mol % of Ni_3C NPs. The powder, partially aggregated at the bottom of the autoclave, was

recovered after reaction by centrifugation and dried under a flux of N_2. Electronic microscopy confirmed the morphology of the NPs has not changed and there seems to be no degradation of the surface (**Figure 6A)**. The corresponding diffractogram, reported in **Figure 6B**, still corresponds to an XRD-pure hcp-Ni_3C phase without substantial evolution. This last result should be compared with blank experiments consisting in the oxidation in air of Ni_3C and Ni(0) NPs powders for 2 h at 250 °C (**Figure S6**). For both phases, most of the XRD signal after calcination was still composed of respectively hcp-Ni_3C and fcc-Ni(0) but small amounts of nickel oxide NiO [PDF card N° 00-047-1049] were observed, presumably at the surface of the NPs. A substantial formation of a nickel oxide shell during catalysis would have therefore been detected by XRD. Finally, XAS spectra were recorded before and after the use of the powder in a catalysis experiment to probe the evolution of the local environment of the Ni atoms. Only small variations were recorded and may be accounted to the normalization process of the spectra (**Figure S7**). The core of the NPs is therefore stable upon catalysis conditions.

The oxidation states of surface nickel and carbon atoms in freshly produced Ni_3C NPs, 6-month-old Ni_3C NPs and *post-mortem* catalyst (reaction in EtOH at 100 °C) were studied by means of X–ray Photoelectron Spectroscopy (XPS) (**Figure 6C-D**). The peak fitting procedure is detailed in the experimental section and was based on reference works.[43]

The Ni $2p_{3/2}$ high-resolution spectra in **Figure 6C** are typically composed of two contributions: reduced Ni(0) in red (one main asymmetric peak with a binding energy (B.E) 852.4 eV) and oxidized Ni^{2+} in green (two main peaks at 855.5 eV and 860.9 eV). The spectra of the Ni $2p_{5/2}$ regions are similar to the Ni $2p_{3/2}$ regions and will not be commented. The spectra of fresh (a) and 6-month-old (b) Ni_3C NPs are very close and display a large contribution of oxidized nickel (NiO, $Ni(OH)_2$…) although a non-negligible proportion of nickel is at a reduced state. Considering the inelastic mean free path (IMFP) of the electrons

(at E_{kin} = 620 eV) is *ca.* 1.0 nm,[44] in contrast with XAS analysis probing the whole nanoparticle, we can conclude that only the extreme surface of the materials got oxidized and that a stable state was reached after an air exposure of a few hours. The Ni_3C NPs after reaction (*post-mortem*) (c) were clearly more reduced with a significant growth of the reduced nickel component when compared with the initial state (b). The catalyst surface was therefore modified upon exposure to H_2 even under mild conditions, *i.e.* at 100 °C in ethanol, potentially due to the *in situ* reduction of residual nickel oxides. One can envision catalytically active sites are composed of reduced nickel atoms. Moreover, to perform the *post-mortem* XPS analysis, the catalyst was washed with EtOH, dried under a flux of N_2 and exposed to air: all these operations were susceptible to oxidize the nickel atoms and the *operando* state of the catalyst is probably even more reduced.

As to the C 1s region (**Figure 6D**), the spectra can be deconvoluted in four components: a yellow component $C_{oxidized}$ at a B.E. of 288.8 eV, a red component C–C (sp^3) at 285.4 eV, an orange component C–C (sp^2) at 284.8 eV (asymmetric peak), and a black component C–Ni at 283.3 eV. This last component is attributed to the carbidic carbons in the Ni_3C structure, with a B.E. in agreement with literature.[45] It is absent of the C 1s spectrum of the Ni(0) NPs (**Figure S8**). The two components C–C (sp^3) and C–C (sp^2) correspond to adventitious carbon and carbon-containing ligands from synthesis: they comport several contributions which may be referred to as sp^2- and sp^3-hybridized carbons. The higher B.E. peak $C_{oxidized}$ may be attributed to surface carbonates formed upon exposure to atmospheric CO_2 or to residual ligands originating from the synthesis in organic solvents, as demonstrated elsewehere.[31] The carbidic component (in black) is undoubtedly present in the *post-mortem* sample, indicating that the carbide phase is preserved even at the extreme surface of the NPs upon catalytic conditions.

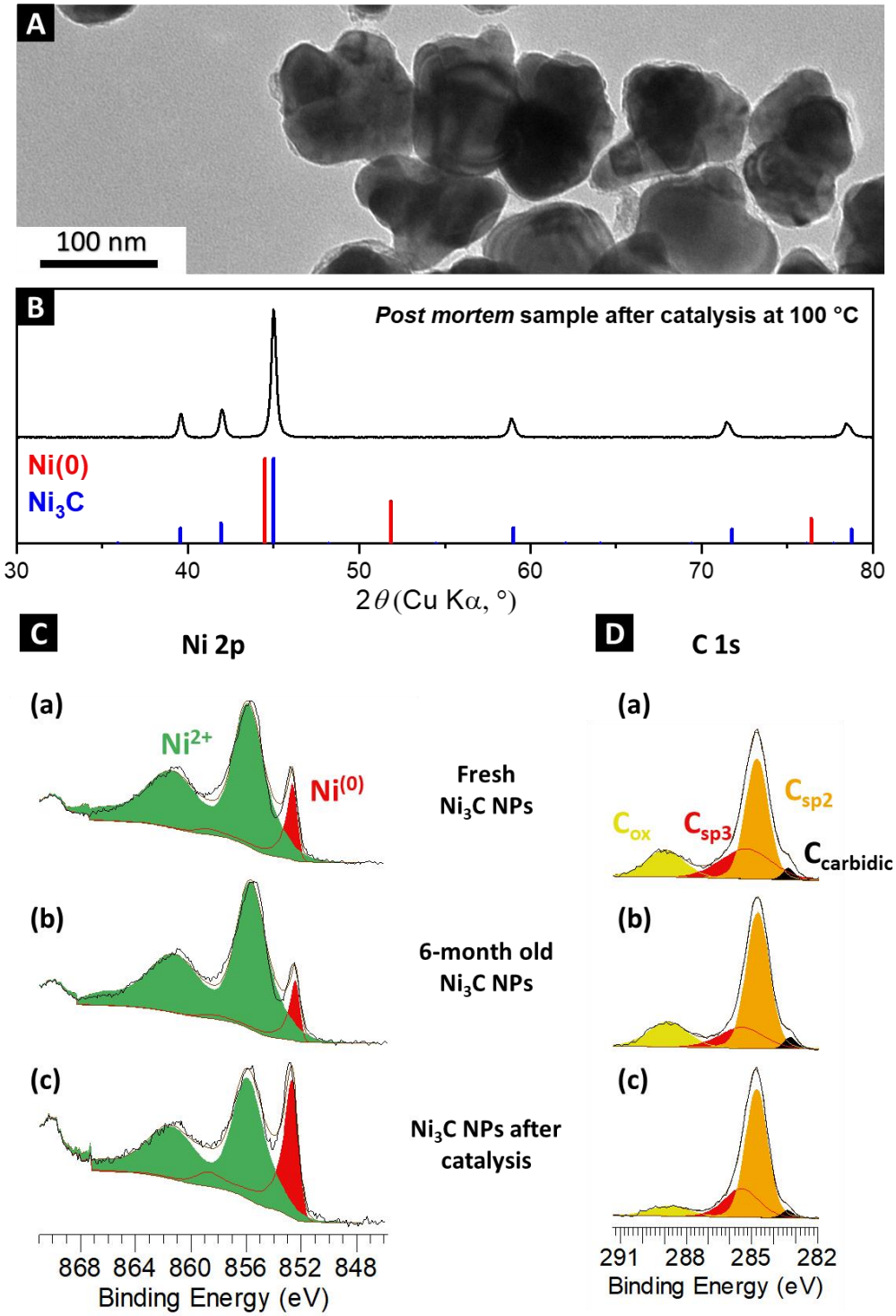

Figure 6. Structural integrity of the catalyst. (A) TEM image and (B) X–Ray Diffractogram of Ni_3C NPs after hydrogenation of phenylacetylene at 100 °C in ethanol. XPS spectra of the (C) Ni 2p and (D) C 1s regions of (a) freshly synthesized Ni_3C NPs, (b) 6-month old Ni_3C NPs, (c) Ni_3C NPs after catalysis at 100 °C.

The integrity of the Ni_3C phase is not trivial as nickel carbide is metastable and decomposes upon heating at higher temperatures. Li *et al.* studied by mass spectrometry and thermal analysis the heating of a powder of Ni_3C nanoparticles under different atmospheres.[46] Under argon (inert atmosphere), Ni_3C decomposed in Ni(0) and amorphous carbon at 415 °C ; under H_2 (reductive atmosphere), it decomposed in Ni(0) and volatile hydrocarbons (methane and ethane) at *ca.* 300 °C ; under air (oxidative atmosphere), it decomposed in NiO and CO_2 above 300 °C. This poor stability at moderate temperatures may be the reason why this phase has been so far overlooked by the catalysis community. Complementarily to this study, our work shows that hcp-Ni_3C nanoparticles are robust during hydrogenation reactions at temperatures up to at least 100 °C and starts oxidizing in NiO before 250 °C if calcined in air.

4. Conclusion

In summary, we presented a simple and robust preparation of hcp nickel carbide (Ni_3C) nanoparticles by decomposition of $Ni(acac)_2$ in OAm and ODE mixture at 250 °C, a temperature that we experimentally justified. The nanoparticles were fully characterized by means of XRD, TEM, XAS and XPS. The obtained material displayed an interesting catalytic activity for the hydrogenation of both unsaturated hydrocarbons and polar groups, with efficiencies equivalent, if not superior, to those of similar metallic fcc-Ni(0) NPs. Different elements were explored to optimize the reaction conditions (solvent, reaction temperature, catalyst loading) and the catalyst was found to be sensitive to NaSCN as a poisoning agent. The integrity of the nanoparticles was finally assessed *via post-mortem* analysis. The reproducible fabrication of this earth-abundant nickel catalyst opens a new route to a possible substitute to platinoids for a number of hydrogenation reactions in fine chemistry. Altogether, this study highlights the interest of hcp-Ni_3C, a catalytic phase so far overlooked for these hydrogenation reactions though active under fairly soft reaction conditions. We hope this will trigger an interest from the heterogeneous catalysis community to develop similar catalysts in supported forms, as well as from the theoretical chemistry community for modeling the active sites, finely evaluating the influence of interstitial carbons and explaining the chemoselectivity we empirically identified.

5. Experimental section

Chemicals. All products were used as received. Oleylamine (OAm) (98 %), 1-octadecene (ODE) (90 %), 1,4-dioxane (98 %), nitrobenzene (99 %), phenylacetylene (98 %), styrene (99 %), benzaldehyde (99.5 %), acetophenone (99 %), naphthalene (99 %), 1-octanal (99 %), 1-octene (98 %), ethyl caprate (99 %), methyl benzoate (98 %), 2-butanone (99 %) and aqueous ammonia (28 %) were purchased from Merck. Absolute ethanol, 1-propanol (98 %), 2-propanol (98 %) and 1-butanol (99 %) were purchased from VWR. $Ni(acac)_2$ (95 %) was purchased from Strem Chemicals. Benzonitrile (99 %) and NaSCN (98 %) were purchased from Alfa Aesar.

Catalyst synthesis. The nickel-containing nanoparticles were prepared *via* a colloidal pathway, according to the literature with some modifications.[30] Typically, in a 100 mL three-necked round-bottom flask, 15 mL of oleylamine (12.2 g, 45.6 mmol, 8.9 equiv.) and 15 mL of 1-octadecene (11.8 g, 46.9 mmol, 9.15 equiv.) were degassed under vacuum at 60 °C during 20 min and the flask was purged with N_2 three times. Under N_2, $Ni(acac)_2$ (1.32 g, 5.14 mmol, 1 equiv.) was added to the solution. The resulting blue gelatinous solution was heated up to 250 °C under stirring. The solution was homogeneous and turned emerald green at 80 °C and darkened progressively with the heating ramp. A black suspension was obtained at 205 °C and explosions occurred at *ca.* 235 °C. The solution was let to react 2 h at 250 °C. After cooling to r.t. under N_2, ethanol (30 mL) was added to the crude solution and a solid was isolated by centrifugation (9,000 rpm, 10 min, 20 °C). The yellow biphasic supernatant was removed and the particles were redispersed in hexane (15 mL) before adding ethanol to precipitate them (15 mL). This operation was repeated another time. The obtained black powder (348 mg, 108 % yield) was then dried under a flux of N_2 and stored under air. The reaction being quantitative,[47] we can expect that *ca.* 10 % of the powder mass is composed of organic species.

Catalyst characterization. Powder X–Ray Diffraction (XRD) measurements were performed on a Bruker D8 Advance diffractometer, using Cu Kα radiation at 1.5406 Å, with steps of 0.05° and a scanning rate of 1°/min. Backgrounds of the patterns are subtracted and heights of the samples are corrected using the EVA software.

For Transmission Electron Microscopy (TEM) analysis, a drop of a diluted solution of nanoparticles dispersed in hexanes was allowed to dry on an amorphous carbon coated copper grid. TEM images were acquired with a TWIN 120 (TECNAI SPIRIT) operating at 120 kV.

X–Ray Photoelectron Spectra (XPS) were collected on an Omicron Argus X–ray photoelectron spectrometer, using a monochromated Al K_α ($h\upsilon$= 1486.6 eV) radiation source having a 300 W electron beam power. The samples were analyzed under ultra-high-vacuum conditions (10^{-8} Pa). After recording a broad range spectrum (pass energy, 100 eV), high-resolution spectra were recorded for the C 1s and Ni 2p core XPS levels (pass energy, 20 eV). The binding energies were calibrated with respect to the C 1s peak at 284.5 eV (graphitic carbon). Spectrum processing was carried out using the CasaXPS software package.

Ni K-edge XAS data were collected at the ROCK beamline at SOLEIL synchrotron, with an electron energy of 2.7 GeV and an average ring current of 500 mA. The incoming photons were selected with a Si (111) monochromator. A 6 mg portion of the sample was diluted in *ca.* 55 mg of graphite and was compressed to form a 10 mm diameter pellet. Spectrum processing was carried out using the Athena software.

Catalytic tests. All catalytic tests were performed in a 25 mL Büchi glass batch reactor. Typically, in air, 12.5 mg of Ni_3C (0.2 mmol, 0.1 equiv. of [Ni]), 1 mL of solvent and 210 μL of nitrobenzene (2 mmol, 1 equiv.) were introduced in the autoclave. The nanoparticles were suspended by sonication during *ca.* 1 min. The autoclave was closed, purged two times with H_2 and pressurized with H_2 to 7 bar (*i.e.* the maximal gas pressure for the system). The autoclave was then introduced in a preheated oil bath at 60 °C or 100 °C for

16 h. The pressure initially increased to *ca*. 8 bar and then decreased to *ca*. 5 bar for full hydrogenation in ethanol. After reaction, the autoclave was let to cool down naturally to r.t. before releasing the pressure. An aliquot of the liquid phase was collected for analysis by ^{1}H NMR in $CDCl_3$ (Bruker Avance-III 300 MHz).

6. List of contributions

R. F. A. conducted the syntheses, the characterizations and the catalysis experiments. L. M. performed preliminary experiments on material synthesis. R. F. A. and S. C. conceived the project and co-wrote the manuscript, S. C. spearheading it. All authors approved the final version of the manuscript.

7. Conflict of interest

The authors declare no conflict of interest.

8. Acknowledgements

This project has received funding from the European Research Council (ERC) under the European Union's Horizon 2020 research and innovation programme (Grant agreement No. 758480). This work was supported by Sorbonne Université and CNRS. This work was supported by a public grant overseen by the French National Research Agency (ANR) as part of the "Investissements d'Avenir" program (reference: ANR 10-EQPX-0045). We acknowledge the ROCK beamline, Valérie Briois and Laurent Barthe at Synchrotron SOLEIL for beamtime (proposal 20201494) for help with the XAS measurements. We acknowledge Antoine Miche for the XPS measurements.

9. References

(1) Delgado, J. A.; Benkirane, O.; Claver, C.; Curulla-Ferré, D.; Godard, C. Advances in the Preparation of Highly Selective Nanocatalysts for the Semi-Hydrogenation of Alkynes Using Colloidal Approaches. *Dalt. Trans.* **2017**, *46* (37), 12381–12403. https://doi.org/10.1039/C7DT01607G.

(2) Vilé, G.; Albani, D.; Almora-Barrios, N.; López, N.; Pérez-Ramírez, J. Advances in the Design of Nanostructured Catalysts for Selective Hydrogenation. *ChemCatChem* **2016**, *8* (1), 21–33. https://doi.org/10.1002/cctc.201501269.

(3) Formenti, D.; Ferretti, F.; Scharnagl, F. K.; Beller, M. Reduction of Nitro Compounds Using 3d-Non-Noble Metal Catalysts. *Chem. Rev.* **2019**, *119* (4), 2611–2680. https://doi.org/10.1021/acs.chemrev.8b00547.

(4) Song, J.; Huang, Z. F.; Pan, L.; Li, K.; Zhang, X.; Wang, L.; Zou, J. J. Review on Selective Hydrogenation of Nitroarene by Catalytic, Photocatalytic and Electrocatalytic Reactions. *Appl. Catal. B Environ.* **2018**, *227* (August 2017), 386–408. https://doi.org/10.1016/j.apcatb.2018.01.052.

(5) Månberger, A.; Johansson, B. The Geopolitics of Metals and Metalloids Used for the Renewable Energy Transition. *Energy Strateg. Rev.* **2019**, *26*, 100394. https://doi.org/10.1016/j.esr.2019.100394.

(6) Raney, M. Method of Producing Finely-Divided Nickel - US1628190A. US1628190A, 1927.

(7) Fouilloux, P. The Nature of Raney Nickel, Its Adsorbed Hydrogen and Its Catalytic Activity for Hydrogenation Reactions (Review). *Appl. Catal.* **1983**, *8* (1), 1–42. https://doi.org/10.1016/0166-9834(83)80051-7.

(8) Roessler, F. Catalytic Hydrogenation in the Liquid Phase. *Chim. Int. J. Chem.* **2003**, *57* (12), 791–798. https://doi.org/10.2533/000942903777678416.

(9) Alexander, A. M.; Hargreaves, J. S. J. Alternative Catalytic Materials: Carbides, Nitrides, Phosphides and Amorphous Boron Alloys. *Chem. Soc. Rev.* **2010**, *39* (11), 4388–4401. https://doi.org/10.1039/b916787k.

(10) Wang, H.; Shu, Y.; Zheng, M.; Zhang, T. Selective Hydrogenation of Cinnamaldehyde to Hydrocinnamaldehyde over SiO_2 Supported Nickel Phosphide Catalysts. *Catal. Letters* **2008**, *124* (3–4), 219–225. https://doi.org/10.1007/s10562-008-9472-y.

(11) Carenco, S.; Leyva-Pérez, A.; Concepción, P.; Boissière, C.; Mézailles, N.; Sanchez, C.; Corma, A. Nickel Phosphide Nanocatalysts for the Chemoselective Hydrogenation of Alkynes. *Nano Today* **2012**, *7* (1), 21–28. https://doi.org/10.1016/j.nantod.2011.12.003.

(12) Gao, R.; Pan, L.; Wang, H.; Zhang, X.; Wang, L.; Zou, J.-J. Ultradispersed Nickel Phosphide on Phosphorus-Doped Carbon with Tailored d-Band Center for Efficient and Chemoselective Hydrogenation of Nitroarenes. *ACS Catal.* **2018**, *8* (9), 8420–8429. https://doi.org/10.1021/acscatal.8b02091.

(13) Yamaguchi, S.; Fujita, S.; Nakajima, K.; Yamazoe, S.; Yamasaki, J.; Mizugaki, T.; Mitsudome, T. Air-Stable and Reusable Nickel Phosphide Nanoparticle Catalyst for the Highly Selective Hydrogenation of d-Glucose to d-Sorbitol. *Green Chem.* **2021**, *23* (5), 2010–2016. https://doi.org/10.1039/D0GC03301D.

(14) Cao, F.; Liu, R.; Zhou, L.; Song, S.; Lei, Y.; Shi, W.; Zhao, F.; Zhang, H. One-Pot Synthesis of Flowerlike Ni_7S_6 and Its Application in Selective Hydrogenation of Chloronitrobenzene. *J. Mater. Chem.* **2010**, *20* (6), 1078–1085. https://doi.org/10.1039/B916866D.

(15) Wei, Z.; Mao, S.; Sun, F.; Wang, J.; Mei, B.; Chen, Y.; Li, H.; Wang, Y. The Synergic Effects at the Molecular Level in CoS_2 for Selective Hydrogenation of Nitroarenes. *Green Chem.* **2018**, *20* (3), 671–679. https://doi.org/10.1039/C7GC03122J.

(16) Shi, X.; Wen, X.; Nie, S.; Dong, J.; Li, J.; Shi, Y.; Zhang, H.; Bai, G. Fabrication of Ni_3N Nanorods Anchored on N-Doped Carbon for Selective Semi-Hydrogenation of Alkynes. *J. Catal.* **2020**, *382*, 22–30. https://doi.org/10.1016/j.jcat.2019.12.005.

(17) Ryabchuk, P.; Agostini, G.; Pohl, M.-M.; Lund, H.; Agapova, A.; Junge, H.; Junge, K.; Beller, M. Intermetallic Nickel Silicide Nanocatalyst—A Non-Noble Metal–Based General Hydrogenation Catalyst. *Sci. Adv.* **2018**, *4* (6), eaat0761. https://doi.org/10.1126/sciadv.aat0761.

(18) Collins, D. J.; Smith, A. D.; Davis, B. H. Hydrogenation of Nitrobenzene over a Nickel Boride Catalyst. *Ind. Eng. Chem. Prod. Res. Dev.* **1982**, *21* (2), 279–281. https://doi.org/10.1021/i300006a016.

(19) Phimsen, S.; Kiatkittipong, W.; Yamada, H.; Tagawa, T.; Kiatkittipong, K.; Laosiripojana, N.; Assabumrungrat, S. Nickel Sulfide, Nickel Phosphide and Nickel Carbide Catalysts for Bio-Hydrotreated Fuel Production. *Energy Convers. Manag.* **2017**, *151*, 324–333. https://doi.org/10.1016/j.enconman.2017.08.089.

(20) Zhang, T.; Guo, X.; Zhao, Z. Glucose-Assisted Preparation of a Nickel–Molybdenum Carbide Bimetallic Catalyst for Chemoselective Hydrogenation of Nitroaromatics and Hydrodeoxygenation of m -Cresol. *ACS Appl. Nano Mater.* **2018**, *1* (7), 3579–3589. https://doi.org/10.1021/acsanm.8b00735.

(21) Smirnov, A. A.; Geng, Z.; Khromova, S. A.; Zavarukhin, S. G.; Bulavchenko, O. A.; Saraev, A. A.; Kaichev, V. V.; Ermakov, D. Y.; Yakovlev, V. A. Nickel Molybdenum Carbides: Synthesis, Characterization, and Catalytic Activity in Hydrodeoxygenation of Anisole and Ethyl Caprate. *J. Catal.* **2017**, *354*, 61–77. https://doi.org/10.1016/j.jcat.2017.07.009.

(22) Shilov, I.; Smirnov, A.; Bulavchenko, O.; Yakovlev, V. Effect of Ni–Mo Carbide Catalyst Formation on Furfural Hydrogenation. *Catalysts* **2018**, *8* (11), 560.

https://doi.org/10.3390/catal8110560.

(23) Bretzler, P.; Huber, M.; Nickl, S.; Köhler, K. Hydrogenation of Furfural by Noble Metal-Free Nickel Modified Tungsten Carbide Catalysts. *RSC Adv.* **2020**, *10* (46), 27323–27330. https://doi.org/10.1039/D0RA02003F.

(24) Hao, J.; Zhang, G.; Zheng, Y.; Luo, W.; Jin, C.; Wang, R.; Wang, Z.; Zheng, W. Controlled Synthesis of Ni_3C/Nitrogen-Doped Carbon Nanoflakes for Efficient Oxygen Evolution. *Electrochim. Acta* **2019**, *320*, 134631. https://doi.org/10.1016/j.electacta.2019.134631.

(25) Fan, H.; Yu, H.; Zhang, Y.; Zheng, Y.; Luo, Y.; Dai, Z.; Li, B.; Zong, Y.; Yan, Q. Fe-Doped Ni_3C Nanodots in N-Doped Carbon Nanosheets for Efficient Hydrogen-Evolution and Oxygen-Evolution Electrocatalysis. *Angew. Chemie Int. Ed.* **2017**, *56* (41), 12566–12570. https://doi.org/10.1002/anie.201706610.

(26) Fan, X.; Peng, Z.; Ye, R.; Zhou, H.; Guo, X. M_3C (M: Fe, Co, Ni) Nanocrystals Encased in Graphene Nanoribbons: An Active and Stable Bifunctional Electrocatalyst for Oxygen Reduction and Hydrogen Evolution Reactions. *ACS Nano* **2015**, *9* (7), 7407–7418. https://doi.org/10.1021/acsnano.5b02420.

(27) Wang, H.; Cao, Y.; Zou, G.; Yi, Q.; Guo, J.; Gao, L. High-Performance Hydrogen Evolution Electrocatalyst Derived from Ni_3C Nanoparticles Embedded in a Porous Carbon Network. *ACS Appl. Mater. Interfaces* **2017**, *9* (1), 60–64. https://doi.org/10.1021/acsami.6b14393.

(28) Zhang, H.; Luo, Z.; Liu, Y.; Jiang, Y. Noble-Metal-Free Ni_3C as Co-Catalyst on $LaNiO_3$ with Enhanced Photocatalytic Activity. *Appl. Catal. B Environ.* **2020**, *277*, 119166. https://doi.org/10.1016/j.apcatb.2020.119166.

(29) Roblero, J. G.; Pola-Albores, F.; Valenzuela, M. A.; Rojas-García, E.; Ríos-Valdovinos, E.; Valverde-Aguilar, G. Ni and Ni_3C Catalysts Supported on Mesoporous

Silica for Dry Reforming of Methane. *Int. J. Hydrogen Energy* **2019**, *44* (21), 10473–10483. https://doi.org/10.1016/j.ijhydene.2019.02.119.

(30) Sarac, M. F.; Wu, W.; Tracy, J. B. Control of Branching in Ni_3C_{1-x} Nanoparticles and Their Conversion into $Ni_{12}P_5$ Nanoparticles. *Chem. Mater.* **2014**, *26* (10), 3057–3064. https://doi.org/10.1021/cm4034353.

(31) Carenco, S.; Boissière, C.; Nicole, L.; Sanchez, C.; Le Floch, P.; Mézailles, N. Controlled Design of Size-Tunable Monodisperse Nickel Nanoparticles. *Chem. Mater.* **2010**, *22* (4), 1340–1349. https://doi.org/10.1021/cm902007g.

(32) Schaefer, Z. L.; Weeber, K. M.; Misra, R.; Schiffer, P.; Schaak, R. E. Bridging hcp-Ni and Ni_3C via a Ni_3C_{1-x} Solid Solution: Tunable Composition and Magnetism in Colloidal Nickel Carbide Nanoparticles. *Chem. Mater.* **2011**, *23* (9), 2475–2480. https://doi.org/10.1021/cm200410s.

(33) Leng, Y.; Shao, H.; Wang, Y.; Suzuki, M.; Li, X. A New Method to Synthesize Nickel Carbide (Ni_3C) Nanoparticles in Solution. *J. Nanosci. Nanotechnol.* **2006**, *6* (1), 221–226. https://doi.org/10.1166/jnn.2006.17934.

(34) Goto, Y.; Taniguchi, K.; Omata, T.; Otsuka-Yao-Matsuo, S.; Ohashi, N.; Ueda, S.; Yoshikawa, H.; Yamashita, Y.; Oohashi, H.; Kobayashi, K. Formation of Ni_3C Nanocrystals by Thermolysis of Nickel Acetylacetonate in Oleylamine: Characterization Using Hard X-Ray Photoelectron Spectroscopy. *Chem. Mater.* **2008**, *20* (12), 4156–4160. https://doi.org/10.1021/cm703644x.

(35) Struis, R. P. W. J.; Bachelin, D.; Ludwig, C.; Wokaun, A. Studying the Formation of Ni_3C from CO and Metallic Ni at T = 265 °C in Situ Using Ni K-Edge X-Ray Absorption Spectroscopy. *J. Phys. Chem. C* **2009**, *113* (6), 2443–2451. https://doi.org/10.1021/jp809409c.

(36) Ricbard Brundle, C.; Evans Charles A., J.; Shaun, W. *Encyclopedia of Materials*

Characterization; Elsevier, 1992. https://doi.org/10.1016/C2009-0-26077-6.

(37) Westerhaus, F. A.; Jagadeesh, R. V.; Wienhöfer, G.; Pohl, M.-M.; Radnik, J.; Surkus, A.-E.; Rabeah, J.; Junge, K.; Junge, H.; Nielsen, M.; Brückner, A.; Beller, M. Heterogenized Cobalt Oxide Catalysts for Nitroarene Reduction by Pyrolysis of Molecularly Defined Complexes. *Nat. Chem.* **2013**, *5* (6), 537–543. https://doi.org/10.1038/nchem.1645.

(38) Li, M.; Chen, S.; Jiang, Q.; Chen, Q.; Wang, X.; Yan, Y.; Liu, J.; Lv, C.; Ding, W.; Guo, X. Origin of the Activity of Co–N–C Catalysts for Chemoselective Hydrogenation of Nitroarenes. *ACS Catal.* **2021**, *11* (5), 3026–3039. https://doi.org/10.1021/acscatal.0c05479.

(39) Deng, Y.; Gao, R.; Lin, L.; Liu, T.; Wen, X.-D.; Wang, S.; Ma, D. Solvent Tunes the Selectivity of Hydrogenation Reaction over α-MoC Catalyst. *J. Am. Chem. Soc.* **2018**, *140* (43), 14481–14489. https://doi.org/10.1021/jacs.8b09310.

(40) Frogneux, X.; Borondics, F.; Lefrançois, S.; D'Accriscio, F.; Sanchez, C.; Carenco, S. Surprisingly High Sensitivity of Copper Nanoparticles toward Coordinating Ligands: Consequences for the Hydride Reduction of Benzaldehyde. *Catal. Sci. Technol.* **2018**, *8* (19), 5073–5080. https://doi.org/10.1039/C8CY01516C.

(41) Palazzolo, A.; Carenco, S. Phosphines Modulating the Catalytic Silane Activation on Nickel–Cobalt Nanoparticles, Tentatively Attributed to Frustrated Lewis Pairs in a Colloidal Solution. *Chem. Mater.* **2021**, *33* (19), 7914–7922. https://doi.org/10.1021/acs.chemmater.1c03105.

(42) Goodman, D. W. Model Catalytic Studies over Metal Single Crystals. *Acc. Chem. Res.* **1984**, *17* (5), 194–200. https://doi.org/10.1021/ar00101a007.

(43) Biesinger, M. C.; Payne, B. P.; Grosvenor, A. P.; Lau, L. W. M.; Gerson, A. R.; Smart, R. S. C. Resolving Surface Chemical States in XPS Analysis of First Row Transition

Metals, Oxides and Hydroxides: Cr, Mn, Fe, Co and Ni. *Appl. Surf. Sci.* **2011**, *257* (7), 2717–2730. https://doi.org/10.1016/j.apsusc.2010.10.051.

(44) Tanuma, S.; Powell, C. J.; Penn, D. R. Calculation of Electron Inelastic Mean Free Paths (IMFPs) VII. Reliability of the TPP-2M IMFP Predictive Equation. *Surf. Interface Anal.* **2003**, *35* (3), 268–275. https://doi.org/10.1002/sia.1526.

(45) Furlan, A.; Lu, J.; Hultman, L.; Jansson, U.; Magnuson, M. Crystallization Characteristics and Chemical Bonding Properties of Nickel Carbide Thin Film Nanocomposites. *J. Phys. Condens. Matter* **2014**, *26* (41), 415501. https://doi.org/10.1088/0953-8984/26/41/415501.

(46) Leng, Y.; Xie, L.; Liao, F.; Zheng, J.; Li, X. Kinetic and Thermodynamics Studies on the Decompositions of Ni_3C in Different Atmospheres. *Thermochim. Acta* **2008**, *473* (1–2), 14–18. https://doi.org/10.1016/j.tca.2008.04.003.

(47) Carenco, S.; Labouille, S.; Bouchonnet, S.; Boissière, C.; Le Goff, X.-F.; Sanchez, C.; Mézailles, N. Revisiting the Molecular Roots of a Ubiquitously Successful Synthesis: Nickel(0) Nanoparticles by Reduction of [Ni(Acetylacetonate)$_2$]. *Chem. - A Eur. J.* **2012**, *18* (44), 14165–14173. https://doi.org/10.1002/chem.201201071.

Table of Content Graphic